# Three-Dimentional Surface Light Irradiance Reconstruction in Bioluminescence Tomography

*Chen Chunxiao*(陈春晓)[1*], *Liu Gao*(刘高)[1], *Zhang Qian*(张倩)[1],
*Li Tingting*(李婷婷)[1], *Wang Zhengsheng*(王正盛)[2], *Li Ning*(黎宁)[3]

1. College of Automation Engineering, Nanjing University of Aeronautics and Astronautics, Nanjing, 210016, P. R. China;
2. College of Science, Nanjing University of Aeronautics and Astronautics, Nanjing, 210016, P. R. China;
3. College of Electronic and Information Engineering, Nanjing University of Aeronautics and Astronautics, Nanjing, 210016, P. R. China

(Received 19 May 2014; revised 5 September 2014; accepted 10 September 2014)

**Abstract**: Reconstruction of 3D surface irradiance distribution using multiple views captured by charged coupled device (CCD) camera is the basis of solving the light source in bioluminescence tomography (BLT). A simple and convenient mapping technique based on the pin-hole imaging model and Lambert's cosine law was presented to establish the relationship between gray levels and irradiance intensities. Compared with previous integrating sphere camera calibration used in BLT, the proposed method can effectively avoid heavy burden of simulation experiment to obtain the corresponding relationship of gray levels and irradiance intensities. The accuracy and feasibility of the proposed method are validated with no more than 1 mm location error by different types of phantom experiments. The mapping approach is also applicable to other noncontact optical imaging system.

**Key words**: light propagation model; irradiance reconstruction; bioluminescence tomography (BLT); pin-hole imaging

**CLC number**: TN21 **Document code**: A **Article ID**: 1005-1120(2014)06-0652-08

## 1 Introduction

Bioluminescence tomography (BLT) is an emerging detection technology at the cellular, molecular, and genetic levels, and has played an important role in the early detection of cancer and therapeutic efficacy evaluation of new drugs[1-3]. BLT attracts a lot of attentions in recent years because of its significant advantages on sensibility, safety, easy operation and less cost[4-5]. In the noncontact optical imaging, accurately obtaining the photon distribution on the surface of the animal is the foundation of light source reconstruction inside the body[6].

Highly sensitive and low noise charged coupled device (CCD) camera and small aperture lenses are often used to acquire the light irradiance distribution on the specimen surface[7-8]. However, photon propagation simulation in free-space is still a challenge. The collected images from CCD only indirectly reflect the irradiance distribution, and need to be turned from gray level value into the corresponding light irradiance intensity. For a selected wavelength, gray levels can be mapped with varying intensity values by using a calibrated integrating sphere[9]. In order to improve the mapping accuracy, Liu, et al.[10] considered the field of view and the distance in their experiments. The projecting system of integrating sphere based on uniform source is expensive and requires a series of tests to build the relationship of the irradiance and the gray level. Schulz and

**Foundation items**: Supported by the National Natural Science Foundation of China (61171059); the Fundamental Research Funds for the Central Universities of China (NP2012202, NZ2014101); the Foundation of Graduate Innovation Center in Nanjing University of Aeronautics and Astronautics(kfjj201427).

* **Corresponding author**: Chen Chunxiao, Professor, E-mail: ccxbme@nuaa.edu.cn.

Ripoll presented a theoretical approach for modeling the noncontact optical measurements and retrieving the 3D surface information of the diffuse medium by means of Green's theorem[11-12]. Combining Lambert's cosine law and the radiance theorem, noncontact optical imaging model was improved, and photon propagation in free space based on hybrid radiosity-radiance theorem was proposed to count 3D distribution of light intensity from images[13-14]. By modeling the camera lens as a combination of a thin lens and a camera lens diaphragm, simulation of the photon transport process was more accurate[15]. Considering the current methods, projecting complication, time-consuming, and mapping accuracy still need improvement.

In this study, a simple and convenient method based on imaging principle of CCD and pin-hole propagating model of the photon in the free space is investigated to establish the congruent relationship between gray level values of the image captured by CCD camera and the light irradiance distribution on 3D surface of the specimen.

## 2 Light Irradiance Reconstruction Method

In BLT, photon propagation includes two sections, namely transmits inside the object and outside the object. The first section means the photon propagating through medium which can be accurately described by the radioactive transport equation (RTE). In order to alleviate the complexity of the RTE, several approximations have been suggested using the spherical harmonics equations[16]. In these approximation methods, the diffusion approximation (DA) is one of the most widely-used forward models, and the finite element method is used to solve the diffusion equation and get the relation matrix between light source and surface light distribution[17]. The second section includes the photon propagating through the air, the camera lenses and finally reaching the detector plane. Retrieving the 3D surface light irradiance distribution by the images acquired from CCD camera is the focus of this study. Unlike previous reports about the BLT system, camera imaging theory was adopted to investigate the relationship between 3D surface photon irradiance intensities of the object and gray level values in the image.

### 2.1 Image coordinate system

The image coordinate system describes how locations are measured in the image. To reconstruct the photon distribution on the surface of specimen, the camera lens model and coordinate transformation between object and detector plane should be considered.

Most cameras contain multiple lenses which are often characterized by Gaussian thick-lens model with two equivalent refracting surfaces[18]. Normally, the Gaussian thick-lens model can be simplified as a thin-lens model by collapsing the first and the second principal planes when the thickness is negligible compared to the radii of curvature of the lens surfaces. Furthermore, the thin-lens model is geometrically equivalent to a pin-hole model as light propagating in free space[19]. The pin-hole imaging model represents an imaging system by a point aperture placed between the scene and the sensor.

In this study, pin-hole lens model is used to describe the mathematical relationship between the coordinates of a 3D point and its projection onto the image. As shown in Fig. 1, the coordinate system contains specimen, lens, and detector plane. In Fig. 1, the $xoz$ plane is the detector plane and parallel to the pin-hole plane, the ray axis is parallel to $y$-axis, and the $x'y'z'$ represents the specimen coordinate system.

In the process of coordinate transformation, a mark point $M_1$ on the surface center of the specimen is set, ensuring its projecting point $M_2$ is also in the center of the image. Then the projecting relationship of $M_1$ and $M_2$ can be expressed

$$\begin{cases} M_{1x} = M_{2x} \\ M_{1y} = v + u \\ M_{1z} = M_{2z} \end{cases} \tag{1}$$

where $v$ is the image distance and $u$ the object distance. And then the translations $t_x, t_y, t_z$ are given

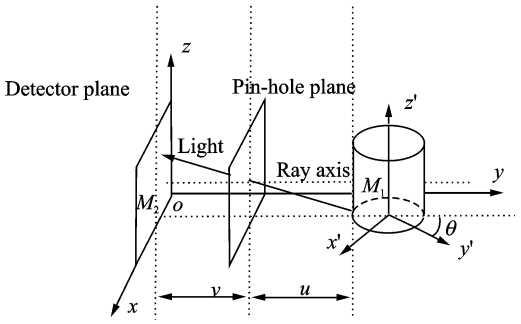


Fig. 1 Light propagation coordinate system

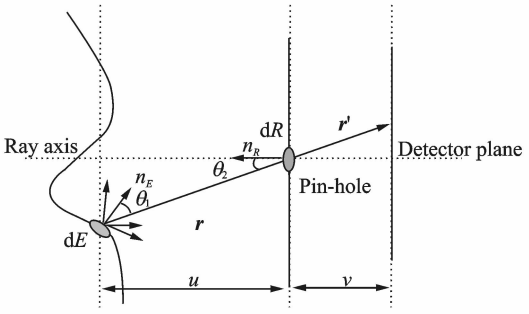


Fig. 2 Light propagation model

$$\begin{aligned} t_x &= M_{1x} - M_{1x'} \\ t_y &= M_{1y} - M_{1y'} \\ t_z &= M_{1z} - M_{1z'} \end{aligned} \tag{2}$$

Therefore, the transformation matrix is shown as[20]

$$\boldsymbol{T} = \begin{bmatrix} \cos\theta & \sin\theta & 0 & 0 \\ -\sin\theta & \cos\theta & 0 & 0 \\ 0 & 0 & 1 & 0 \\ 0 & 0 & 0 & 1 \end{bmatrix} \cdot \begin{bmatrix} 1 & 0 & 0 & t_x \\ 0 & 1 & 0 & t_y \\ 0 & 0 & 1 & t_z \\ 0 & 0 & 0 & 1 \end{bmatrix} \tag{3}$$

where $\theta$ is set as the rotation angle (Fig. 1), $t_x$, $t_y$ and $t_z$ are the coordinate differences of $M_1$ in two coordinate systems.

## 2.2 Light propagation model

In BLT, photon propagation out of the specimen can be modeled as shown in Fig. 2. In Fig. 2, $\boldsymbol{r}$ and $\boldsymbol{r}'$ are defined as vectors from the center point of triangular patch to the pin-hole and from pin-hole to the detector plane, respectively. Photons emitted from differential element d$E$ spread in different directions, but only those photons in $\boldsymbol{r}$ direction will go through the pin-hole and reach the detector plane. Define the light power of differential element d$E$ as d$P$, the photon power of differential element d$R$ crossing the pin-hole as d$P'$, and the photon power reaching the detector plane as d$P''$. When the image distance is far more than that of the aperture of the lens, d$P'$is approximately equal to d$P''$. In accordance with the Lambert's cosine law, the photon power at the detector plane is[21]

$$\mathrm{d}P'' \approx \mathrm{d}P' = \frac{1}{\pi}\mathrm{d}L_E S_E S_R \cos\theta_1 \cos\theta_2 / d_{ER}^2 \tag{4}$$

where d$L_E$ is the light irradiance at the differential element d$E$; $\theta_1$ and $\theta_2$ are indicated in Fig. 2; $S_E$ and $S_R$ the areas of differential elements d$E$ and d$R$, respectively; and $d_{ER}$ the distance between d$E$ and d$R$. Then, the projecting relationship between light irradiance of differential element d$E$ and light power receiving by CCD detector plane is described as follows

$$\mathrm{d}L_E = \frac{\pi \cdot \mathrm{d}P'' d_{ER}^2}{S_E S_R \cos\theta_1 \cos\theta_2} \tag{5}$$

## 2.3 Gray level to light power

CCD camera calibration conducted by the integrating sphere system is commonly used to establish the relationship between gray level value and light power. In order to avoid the use of expensive calibration system, the imaging principle of CCD camera is investigated to obtain the mapping relationship between gray level value and light power. As we know, the CCD converts incoming photons into charges and manifests as gray levels in an image, which satisfies

$$n_p = \frac{AI}{Q_e T_r} \tag{6}$$

where $n_p$ is the number of photons read out by CCD in each pixel and $I$ the gray level of the pixel. The gain $A$, the quantum efficiency $Q_e$, and the transmittance of lens $T_r$ are parameters of the CCD camera.

According to photon energy formula $E = h\nu$, the light power d$P''$ at each pixel is

$$\mathrm{d}P'' = n_p \cdot \frac{h v_p}{\lambda} \cdot \frac{1}{t} \tag{7}$$

where $h$ is the Planck constant, $v_p$ the speed of light, $\lambda$ the wave length, and $t$ the time of exposure.

Based on Eqs. (5－7), the light irradiance on the 3D surface of the specimen can be ex-

pressed as

$$dL_E = \frac{\pi h A V_p d_{ER}^2}{S_E S_R Q_e T_r \lambda t \cos\theta_1 \cos\theta_2} I \tag{8}$$

### 2.4 Light irradiance mapping procedure

In the reconstruction of 3D surface light irradiance in BLT, the volume mesh of the specimen is needed. Each triangular patch of the mesh represents the differential emitting element $dE$, and its corresponding differential receiving element is $dR$ in the image. Actually, one $dE$ may be mapped with more than one $dR$. The whole procedure is demonstrated as follows:

**Step 1** Convert the image coordinate into $xyz$ coordinate system in Fig. 1.

**Step 2** Convert coordinates of mesh nodes into $xyz$ coordinate system using matrix $\boldsymbol{T}$.

**Step 3** Match the triangular patch with corresponding pixel point. Normally, $\boldsymbol{r}$ and $\boldsymbol{r}'$ in Fig. 2 seldom lie on the same straight line. Traversing all vectors $\boldsymbol{r}'$ to certain $\boldsymbol{r}$, the closest to the direction of $\boldsymbol{r}$ is selected, and then the corresponding triangular patch is mapped with this pixel point on the detector plane.

**Step 4** Convert the gray levels of image to irradiance intensities based on Eq. (8).

**Step 5** When more than one pixel point corresponds with the same triangular patch, the irradiance of this patch should be conducted by integral operation.

In order to further evaluate the proposed mapping method, a correlation coefficient is computed by

$$\mathrm{Corr} = \frac{\sum XY - \frac{\sum X \sum Y}{N}}{\sqrt{\left(\sum X^2 - \frac{(\sum X)^2}{N}\right)\left(\sum Y^2 - \frac{(\sum Y)^2}{N}\right)}} \tag{9}$$

where $X$ is the group of light irradiance of surface nodes calculated by DA equation, $Y$ the group of mapping results, and $N$ the number of nodes.

## 3 Materials

Several experiments of different phantoms are employed to prove the validity of the surface irradiance reconstruction method, including a cylindrical nylon phantom, an irregular surface nylon phantom, and a cubic meat phantom. The absorption coefficient $\mu_{an}$ and reduced scattering coefficient $\mu'_{sn}$ of nylon are 0.013 8 $mm^{-1}$ and 0.91 $mm^{-1}$, respectively. $\mu_{am}$ and $\mu'_{sm}$ of meat are 0.23 $mm^{-1}$ and 1 $mm^{-1}$, respectively. The light source is set with a glow stick which spectral range is 600—780 nm, peak value is 650 nm, and luminous intensity is 60 at room temperature[22]. The BLT system contains a CCD camera (Princeton Instruments exclusive PIXIS: 1024B_eXcelon) coupled with a micro camera lens (TAMRON M118FM25), a dark chamber, a translation and rotation platform and several filters. The image size is 1 024 pixel×1 024 pixel, and spatial resolution is 0.013 mm.

In the experiments, luminescent 2D images at different angles are acquired by CCD camera. In experiments of nylon phantoms, eight images at 0°, 45°, 90°, 135°, 180°, 225°, 270°, and 315° are taken. In experiment of meat phantom, four images at 0°, 90°, 180°, and 270° are taken. These images are needed to reconstruct the light source in BLT. Volume mesh of phantom can be obtained by using meshing tools developed in our laboratory.

The whole reconstructing procedure of the algorithm merely takes less than one minute using a Intel(R) Core(TM), 2.6 GHz, 2.00 GB RAM machine with operating system Windows XP, running in Matlab 2012b environment.

## 4 Results and Discussion

### 4.1 Cylindrical nylon phantom experiment

The cylindrical phantom is a nylon stick with 40 mm height and 40 mm diameter. A cylindrical hole with 5 mm diameter and 20 mm height filled with 98 $\mu'_L$ fluorescent liquid is located inside the nylon phantom. The three views of the phantom and its volume mesh are shown in Fig. 3. The phantom consists of 15 331 tetrahedral elements and 2 918 nodes.

Eight views acquired by CCD camera at different angles are shown in Fig. 4. Utilizing the eight images, the light irradiance distributions on

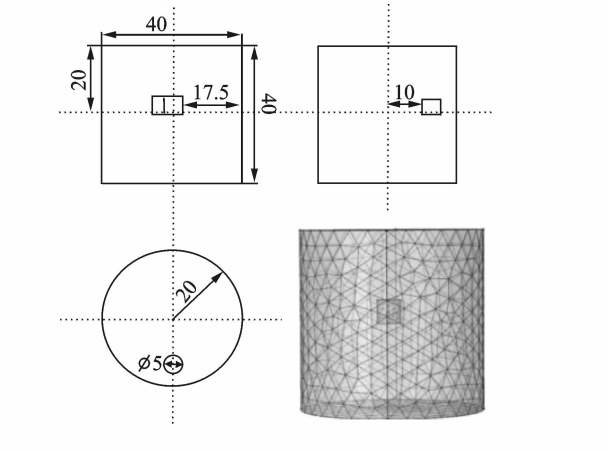


Fig. 3 Three views and volume mesh of cylinder phantom

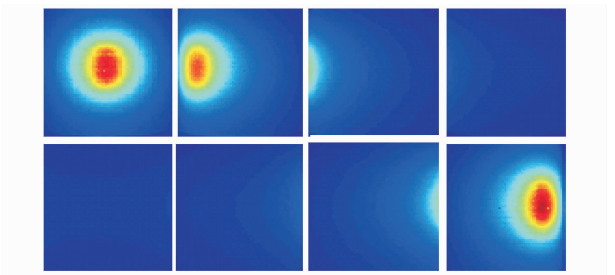

Fig. 4 Eight views of cylinder phantom taken by camera

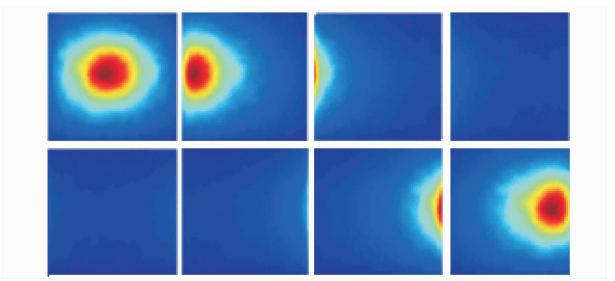

Fig. 5 Eight views irradiance reconstructed by the proposed method

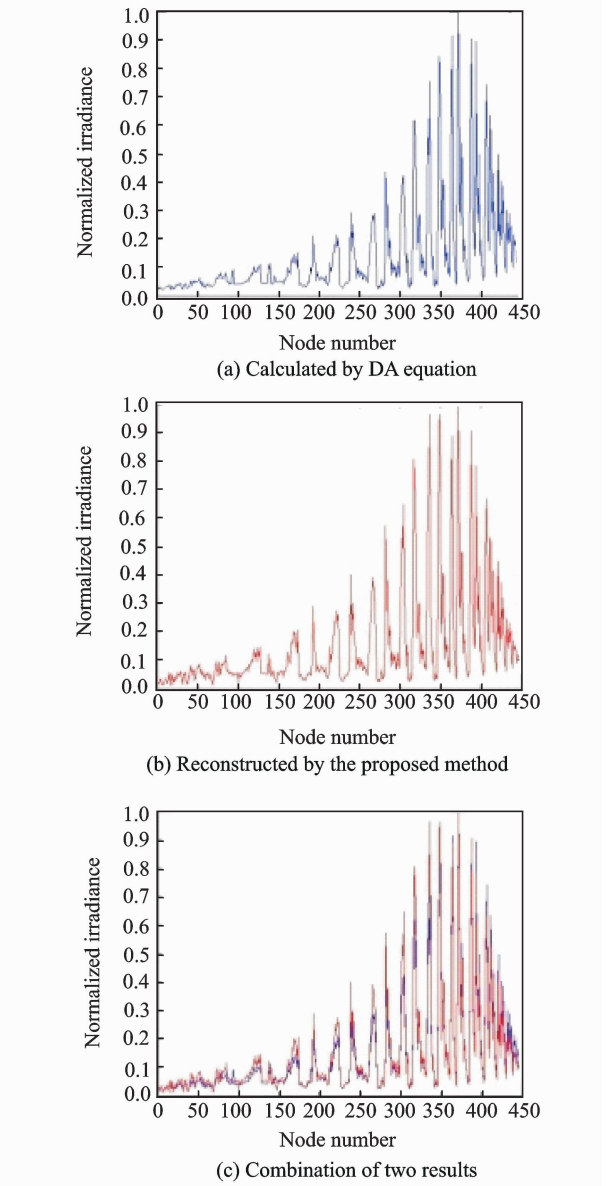


Fig. 6 Comparison of light irradiance of surface nodes by different methods

the cylinder phantom are mapped in Fig. 5.

To verify the accuracy of the mapping method, the correlation coefficient of surface intensities is computed by Eq. (9). Fig. 6(a) represents the light irradiance of surface node calculated by DA equation, while Fig. 6(b) the mapping result of the proposed method. Drawing two results in the same coordinate, Fig. 6(c) indicates their similarities. In this experiment, Corr of $X$ and $Y$ is 0.978 8.

To further demonstrate the correctness of the surface mapping method, we use the light irradiance mapping results to reconstruct the light source inside the phantom. Tikhonov regularization is used to solve the light source for decreasing the ill-posedness of BLT. In Fig. 7, the blue and the red volumes represent the true source and the reconstructed source respectively. The distance error of their source center is 0.40 mm.

### 4.2 Irregular surface nylon phantom experiment

An irregular surface nylon phantom is used to further verify the generality of the mapping algorithm. The size of the light source is the same with that of the first experiment. Three views of the phantom and its volume mesh are shown in Fig. 8. Eight views acquired by CCD camera at different angles are shown in Fig. 9. The phan-

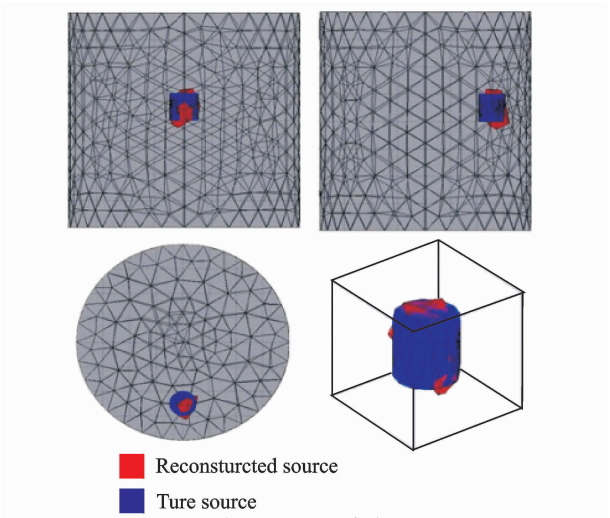


Fig. 7 Three views of the source

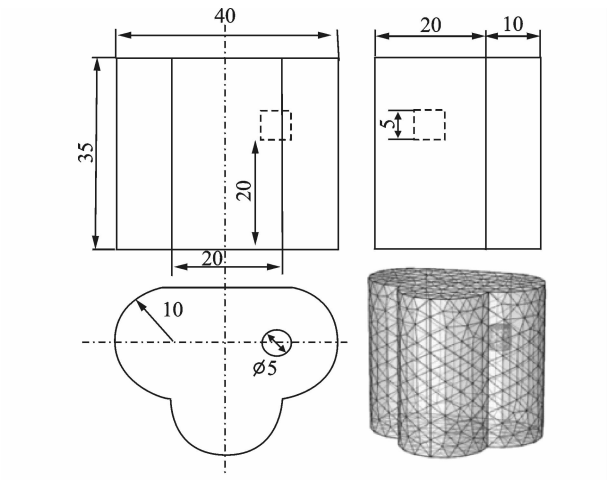


Fig. 8 Three views and volume mesh irregular phantom

tom consists of 15 161 tetrahedral elements and 2 661 nodes.

Reconstruction of the surface light irradiance distribution is shown in Fig. 10. The correlation coefficient of irradiance on the surface nodes between the calculated result by DA equation and the mapping result is 0.953 1. In Fig. 11, the blue and the red volumes represent the true source and there constructed source respectively and the distance error of their source center is 0.48 mm.

### 4.3 Cubic meat phantom experiment

To further validate the mapping algorithm in different kinds of materials, a transparent cylinder pipe filled with fluorescent liquid was buried into a cubic meat phantom. The size of the light source is the same with the first experiment. Three views of the phantom and its volume mesh

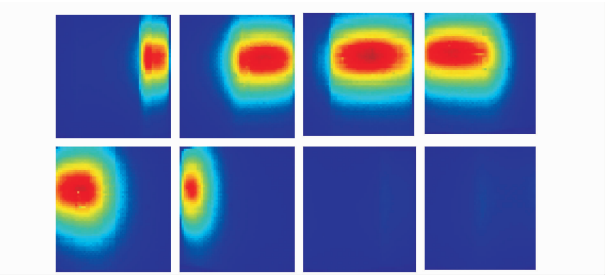

Fig. 9 Eight views taken by CCD camera

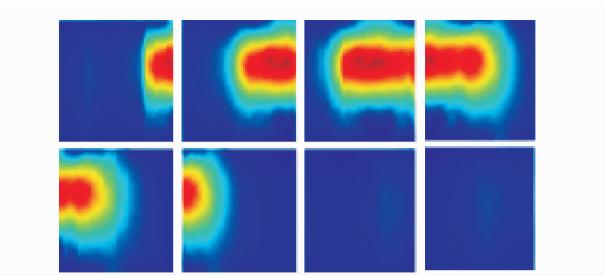

Fig. 10 Eight view irradiance reconstructed by the proposed method

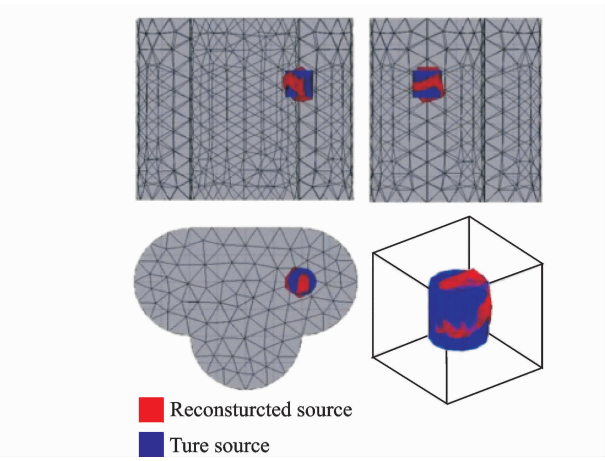


Fig. 11 Three views of source

are shown in Fig. 12. The phantom consists of 12 353 tetrahedral elements and 2 405 nodes. Since this phantom is a cube and its surface is planar, only four-view images need to be acquired by CCD camera from directions with a 90° interval.

One of the views is shown in Fig. 13(a), and the surface irradiance reconstruction is shown in Fig. 13(b). The correlation coefficient of irradiance on the surface nodes between the calculated results by DA equation and the mapping results is 0.964 9. Fig. 14 shows a comparison between gray level values taken by camera and irradiance of each mesh nodes at the height of 15 mm in one view. The values of two groups are normalized.

In Fig. 15, the blue and the red volumes re-

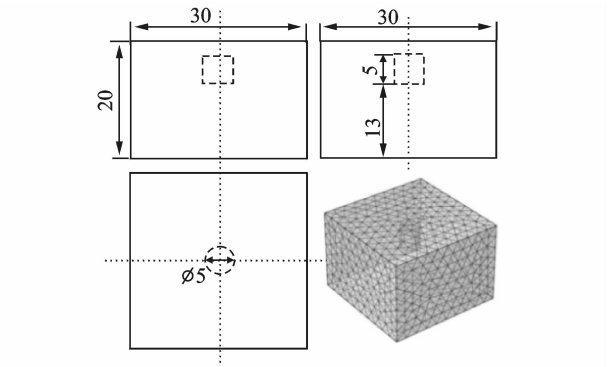


Fig. 12 Three views and volume mesh of cube phantom

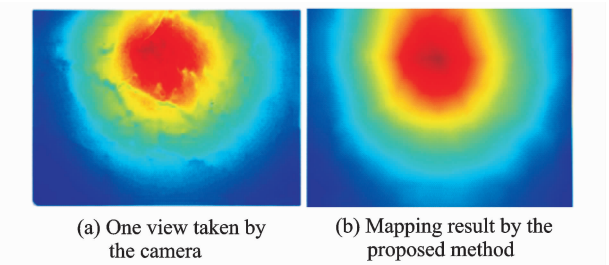


Fig. 13 Image taken by CCD and reconstruction result

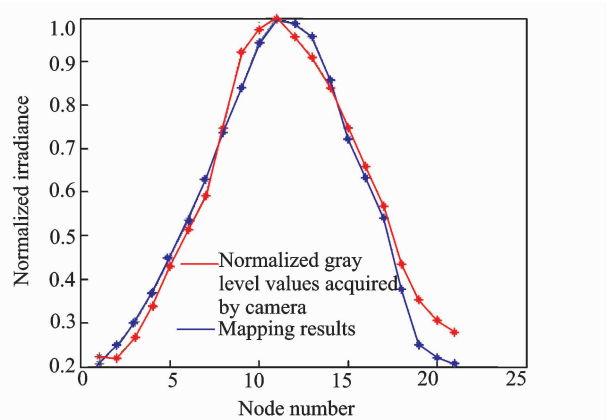


Fig. 14 Comparison of gray level values and irradiances

present the true source and the reconstructed source, respectively. The distance error of their source center is 0.70 mm.

Table 1 shows indexes of surface irradiance and source reconstruction. In Table 1, Corr is the correlation coefficient calculated by Eq. (9), and $D_{err}$ the distance error of center points between the true source and the reconstructed source.

**Table 1 Reconstruction indexes of three experiments**

| Index | Corr | $D_{err}$/mm |
|---|---|---|
| Cylindrical phantom | 0.978 8 | 0.40 |
| Irregular phantom | 0.953 1 | 0.48 |
| Cubic meat phantom | 0.964 9 | 0.70 |

According to Table 1, the correlation coefficients of the photon distribution are all more than 0.95 between reconstructed results and the forward calculation by DA equation. Furthermore, utilizing the mapping results of 3D surface irradiance based on multiple views at different directions, the light sources inside the phantoms are reconstructed, and the location errors are less than 1 mm.

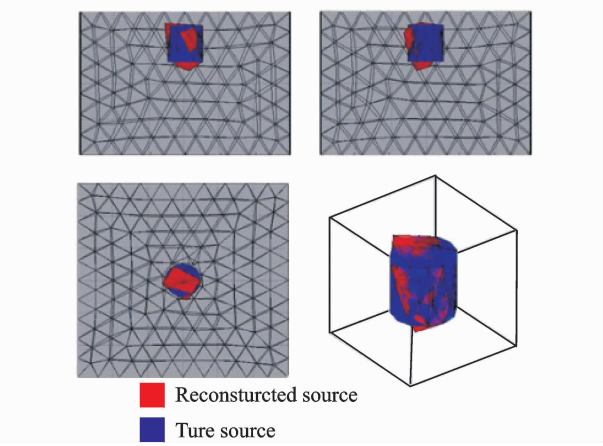


Fig. 15 Three views of source

## 5 Conclusions

A simple and convenient 3D surface light irradiance reconstruction method is presented in this study, which is the basis of accurately solving the light source in BLT. Unlike the previous studies, this reconstruction technique based on the imaging theory of the CCD camera and Lambert's cosine law can be implemented without integrating sphere for calibration. Utilizing the parameters of the CCD camera, such as the gain, the quantum efficiency and the transmittance of lens, the corresponding relationship between gray levels and irradiance intensities are easily established. Three experiments for different types of phantoms are employed to test its validity. It is obvious that the light irradiance distribution reconstructed by the proposed method is quite similar to its real distribution captured by CCD camera.

The preliminary experimental results demonstrate the feasibility and efficacy of the proposed mapping approach. However, this pin-hole mapping model is based on the assumption that the

effective aperture is negligible compared to the radii of curvature of the lens surfaces. Otherwise, if the effective aperture is comparable to the size of the lens, the model should be calibrated. In the future work, the mapping model needs to be further improved, and corresponding results will be reported later. The 3D surface irradiance reconstruction method presented in this paper can also be used in other noncontact optical imaging.

**References:**


[1] Dufort S, Sancey L, Wenk C, et al. Optical small animal imaging in the drug discovery process [J]. Biochimica et Biophysica Acta (BBA)—Biomembranes, 2010, 1798(12): 2266-2273.

[2] Xu H, Zoraida P, Su H, et al. In situ imaging of breast cancer cells using green semiconductor quantum dots [J]. Transactions of Nanjing University of Aeronautics & Astronautics, 2010, 27(1): 13-20.

[3] Tsai H R, Bentz B Z, Chelvam V, et al. In vivo optical imaging of kinetics in a small animal for folate-targeted drug development [C] // Optical Trapping Applications. Hawaii, USA: Optical Society of America, 2013: JW3B. 5.

[4] Tian J, Bai J, Yan X P, et al. Multimodality molecular imaging [J]. Biomedical Engineering in China, 2008, 27(5):48-57.

[5] Qin C, Zhu S, Tian J. New optical molecular imaging systems [J]. Current Pharmaceutical Biotechnology, 2010, 11(6): 620-627.

[6] Tarik F M, Gambhir S S. Molecular imaging in living subjects: seeing fundamental biological processes in a new light [J]. Genes & Development, 2013, 17: 545-580.

[7] Ntziachristos V, Ripoll J, Wang L V, et al. Looking and listening to light: the evolution of whole-body photonic imaging [J]. Nature Biotechnology, 2005, 23(3):313-320.

[8] Nikolaos D, Tobias L, Damon H, et al. Free-space fluorescence molecular tomography utilizing 360° geometry projections [J]. Optics Letters, 2007, 32 (4):382-384.

[9] Cong W, Wang G, Kumar D, et al. Practical reconstruction method for bioluminescence tomography [J]. Optics Express, 2005, 13(18): 6756-6771.

[10] Liu J, Chen D, Li X, et al. In vivo quantitative reconstruction studies of bioluminescence tomography: effects of peak-wavelength shift and model deviation [J]. Biomedical Engineering, IEEE Transactions on, 2010, 57(10): 2579-2582.

[11] Ralf B, Schulz R B, Jorge R, et al. Noncontact optical tomography of turbid media [J]. Optics Letters, 2003, 28 (18):1701-1703.

[12] Ripoll J, Schulz R B, Ntziachristos V, et al. Free space propagation of diffuse light: Theory and experiments [J]. Physics Review Letters, 2003, 91(10): 103901-1-4.

[13] Chen X, Gao X, Qu X, et al. A study of photon propagation in free-space based on hybrid radiosity-radiance theorem [J]. Optics Express, 2009, 17 (18): 16266-16280.

[14] Chen X, Gao X, Chen D, et al. 3D reconstruction of light flux distribution on arbitrary surfaces from 2D multi-photographic images [J]. Optics express, 2010, 18(19): 19876-19893.

[15] Chen X, Gao X, Qu X, et al. Generalized free-space diffuse photon transport model based on the influence analysis of a camera lens diaphragm [J]. Applied Optics, 2010, 49(29): 5654-5664.

[16] Tian J, Liu K, Lu Y, et al. Evaluation of the simplified spherical harmonics approximation in bioluminescence tomography through heterogeneous mouse models [J]. Optics Express, 2010, 18(20): 20988-21002.

[17] Tarvainen T, Vauhkonen M, Kolehmainen V, et al. Finite element model for the coupled radiative transfer equation and diffusion approximation [J]. International Journal for Numerical Methods in Engineering, 2006, 65(3): 383-405.

[18] Kingslake R. Optical system design [M]. [S. l.]: Academic Press, 1983.

[19] Manoj A, Narendra A. A pupil-centric model of image formation [J]. Int J Comput Vis, 2002, 48(3): 195-214.

[20] Klose A D, Beattie B J. Bioluminescence tomography with CT/MRI co-registration [C]// 31st Annual International Conference of the IEEE EMBS. [S. l.]: IEEE, 2009: 6237-6330.

[21] Yao J J, Hu G, Bai J M. Modeling and validation of light propagation in free-space for non-contact near-infrared fluorescent tomography [J]. Infrared Millim Waves, 2008, 27(5): 330-333.

[22] Liu J, Wang Y, Qu X, et al. In vivo quantitative bioluminescence tomography using heterogeneous and homogeneous mouse models [J]. Optics Express, 2010, 18(12): 13102-13113.


(Executive editor: Zhang Bei)